Montelukast photodegradation :

Elucidation of Φ–order kinetics, determination of quantum yields and application to actinometry.

Mounir Maafi*, Wassila Maafi

Leicester School of Pharmacy, De Montfort University, The Gateway, Leicester LE1 9BH, UK

Abstract

A recently developed Φ–order semi–emperical integrated rate–law for photoreversible AB(2Φ) photoreversible reactions has been successfully applied to investigate Montelukast sodium (Monte) photodegradation kinetics in ethanol. The model equations also served to propose a new stepwise kinetic elucidation method valid for any AB(2Φ) system and its application to the determination of Monte forward ($\Phi_{A\rightarrow B}^{\lambda_{irr}}$) and reverse ($\Phi_{B\rightarrow A}^{\lambda_{irr}}$) quantum yields at various irradiation wavelengths. It has been found that $\Phi_{A\rightarrow B}^{\lambda_{irr}}$ undergoes a 15–fold increase with wavelength between 220 and 360 nm, with the spectral section 250 – 360 nm representing Monte effective photodegradation causative range. The reverse quantum yield values were generally between 12 and 54 % lower than those recorded for $\Phi_{A\rightarrow B}^{\lambda_{irr}}$, with the *trans*–isomer (Monte) converts almost completely to its *cis*–counterpart at high irradiation wavelengths. Furthermore, the potential use of Monte as an actinometer has been investigated and an actinometric method was proposed. This study demonstrated the usefulness of Monte for monochromatic light actinometry for the dynamic range 258 – 380nm.

Keywords: Montelukast, photodegradation, spectrokinetics, photoisomerism, actinometry, quantum yield.

Corresponding author. Tel.: +44 116 257 7704; fax: +44 116 257 7287.

E-mail address: mmaafi@dmu.ac.uk (M.Maafi)

1. Introduction

Montelukast sodium (Monte), sodium 1-(1(R)-(3-(2-(7-chloro-2-quinolinyl)-(E)- ethenyl)phenyl) 3-(1-hydroxy-1-methylethyl)phenyl)propyl)thio)methyl) cycloproprane) acetate, is an oral drug used in the treatment of asthma and to relieve the symptoms of seasonal allergies (Schoors et al, 1995). Pharmacologically, it is classed as a leukotriene receptor antagonist since it acts by binding to the cystenyl leukotriene receptor $CysLT_1$ in the lungs and bronchial tubes (Schoors et al, 1995). As such it blocks the action of leukotriene D4 on these receptors thereby reducing bronchoconstriction and inflammation (Schoors et al, 1995).

Monte has been reported to be highly photolabile, especially in solution (Smith et al., 2004). Exposure of this drug even to very low levels of UV radiation, results in its degradation. It obeys a *trans–cis* photoisomerisation mechanism whereby its (*E*)–ethenyl moiety rotates to the (*Z*) geometry (Smith et al., 2004). The overall reaction is labelled here AB(2Φ) as it involves two reversing photochemical reactions between the drug and its photoisomer (Maafi and Maafi, 2014) (Scheme 1).

Thus, special handling precautions were proposed to protect the drug from exposure to light in order to avoid photodegradation, such as by using amber glass vials (Zhao et al., 1997), wrapping with black paper (Radhakrishna et al., 2003) or aluminium foil paper (Thibert et al., 1996) and storage in the dark, or analysis under amber/red light conditions (Arison et al., 1999).

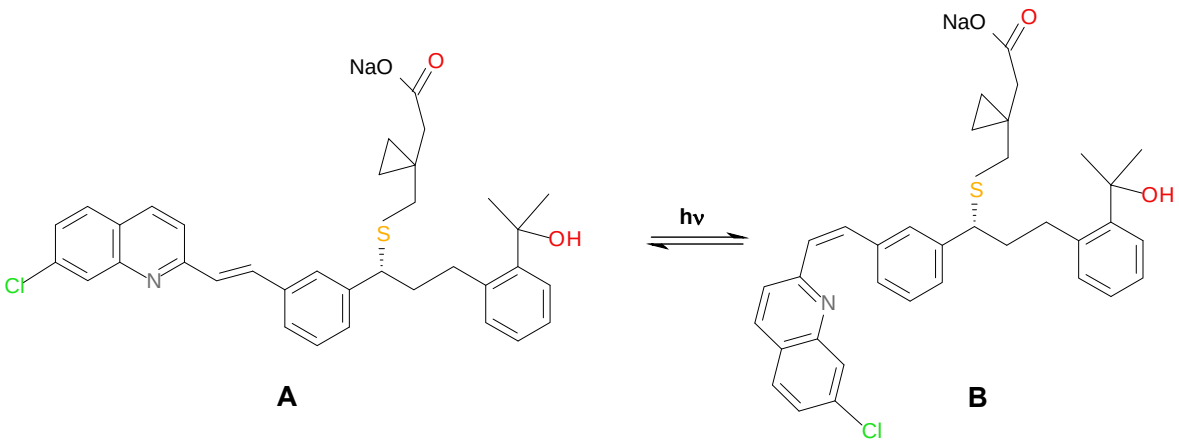

Scheme 1. *Trans* to *cis* photoisomerism of Monte upon exposure to UV–irradiation.

The kinetic studies that have been conducted on Monte photodegradation have employed classical thermal kinetic models and found it to obey either the zeroth or first–order kinetics (Roman et al., 2011; Alsarra, 2004; Al Omari et al., 1999). However, to the best of our knowledge, no attempts have so far been devoted to determining the quantum yields of Monte photodegradation. This is the case for a number of AB(2Φ) photoreversible drugs including some antipsychotics, tricyclic antidepressants, cephalosporin antibiotics, and corticosteroids (Ming, 2012).

In fact, the lack of quantum yields' determination is common for a ubiquitous number of AB(2Φ) photoreversible systems used in the pharmaceutical field despite the fact that such systems have found a wide range of applications in numerous research areas ranging from photodynamic materials and photo–nanomedicine (Fomina et al, 2012; Feliciano et al, 2010) to photoresponsive hydrogels and polymeric capsules (Wohl and Engbersen, 2012; Tomatsu et al, 2011). Research in targeted drug delivery, for instance, has recently turned its attention towards triggered drug delivery through the use of stimuli-responsive delivery devices (Fomina

et al, 2012; Wohl and Engebersen, 2012; Tomatsu et al, 2011; Feliciano et al, 2010). Light–stimulus represents a particularly attractive means which is currently being actively explored as it can be remotely applied and controlled in space and time thereby affording more precise control over drug release site and dosage (Fomina et al, 2012; Tomatsu et al, 2011). In general, a number of advantages are procured by these delivery devices, including a reduction of undesirable side effects, higher drug levels reaching the target sites, enhanced *in vivo* action, reduced drug degradation and a precise control over dosage regimen (Fomina et al, 2012; Tomatsu et al, 2011). It therefore becomes imperative for the design and/or application of such photoreversible systems to have an accurate knowledge of the photoreactions' attributes and their photokinetic behaviour.

In a recent study (Maafi and Maafi, 2014) it has been shown that AB(2Φ) systems obeyed Φ–order kinetics as does the unimolecular AB(1Φ) nifedipine photodegradation (Maafi and Maafi, 2013). These new kinetic treatments overcome the drawbacks of the classical procedures by not only providing a specific mathematical framework to deal with photodegradation reactions (replacing the integrated rate–laws developed for thermal reactions (Piechocki and Thoma, 2010)) but also by allowing better and more reliable insight into the reactions' kinetic behaviour and physico–chemical attributes.

The aim of this study was to investigate Monte kinetics and to propose a new method for the elucidation of the Φ–order kinetics using Monte as an example for AB(2Φ) systems. The strategy is further employed in determining wavelength–dependent values for the reaction's

95 forward and reverse quantum yields. Finally, the potential of the mathematical framework is
96 put to advantage towards demonstrating the usefulness of Monte in actinometry.

97

98 **2. Materials and methods**

99

100 2.1. *Materials*

101 Montelukast sodium, 2-[1-(R)-[3-[2(*E*)-(7-chloroquinolin-2-yl)vinyl]phenyl]-3-[2-(1-hydroxy-1-
102 methylethyl)phenyl]propyl-sulfanylmethyl] cyclopropyl] acetic acid sodium salt (Monte), and
103 spectrophotometric grade ethanol were purchased from Sigma-Aldrich.

104

105 *2.2. Monochromatic continuous irradiation*

106

107 For irradiation experiments, a Ushio 1000 W xenon arc-lamp light source housed in a housing
108 shell model A6000 and powered by a power supply model LPS–1200, was used. This setting was
109 cooled by tap water circulation through a pipe system. The lamp housing was connected to a
110 monochromator model 101 that allows the selection of specific irradiation wavelenghths since
111 it consists of a special f/2.5 monochromator with a 1200 groove/300nm blaze grating. The
112 excitation beam was guided through an optical fibre to impinge from the top of the sample
113 cuvette i.e. the excitation and the analysis light beams were perpendicular to each other. The
114 set up was manufactured by Photon Technology International Corporation.

115

2.3. The monitoring system

A diode array spectrophotometer (Agilent 8453) was used to measure the various absorption spectra and kinetic profiles for the irradiation and calibration experiments. This spectrophotometer was equipped with a 1-cm cuvette sample holder and a Peltier system model Agilent 8453 for temperature control. As such, the sample was kept at 22°C, stirred continuously during the experiment, and almost completely shielded from ambient light. The spectrophotometer was monitored by an Agilent 8453 Chemstation kinetics–software.

A Radiant Power/Energy meter model 70260 was used to measure the radiant power of the incident excitation beams.

2.4. Kinetic data treatment

In order to carry out non–linear fittings and to determine best-fit curves, a Levenberg-Marquardt iterative program within the Origin 6.0 software was used.

2.5. HPLC measurements

The HPLC system consisted of a reversed-phase Jupiter 5µ C-18 300A Phenomenex (250 x 4.60 mm) column equipped with Perkin Elmer Series 200 pump, UV/Vis detector, vacuum degasser and a Perkin Elmer type Chromatography Interface 600 series Link linked to a computer system.

The mobile phase consisted of 15 % water adjusted to pH 3.18 with glacial acetic acid and 85 % methanol. A flow rate of 1 ml/min and an injection loop of 20 μl were used. The detector wavelength was set at 254 nm.

2.6. Monte solutions

A 7.4 x 10^{-4} M stock solution of Monte in ethanol was prepared by weighing the solid. The flask was protected from light by aluminium foil wrapping and was kept in the fridge. The stock solution was diluted to prepare fresh analytical solutions (*ca.* 2 x 10^{-6} M) for analysis of irradiation experiments performed at various wavelengths.

For actinometric studies, Monte solutions of the same concentrations (*ca.* 2 x 10^{-6} M) were exposed to specific wavelengths irradiations (258, 328, 345 and 360 nm) using a series of different intensities for each wavelength. The kinetic traces were observed at the irradiation wavelength and subsequently fitted with the Φ–order equations.

Experiments were conducted at least in triplicates.

3. Results and discussion

3.1. The Mathematical background

The differential equation (Eq.1) expressing the time variation of the concentrations of species A and B (C_A(t) and C_B(t), respectively), considering that the solution, being subjected to a monochromatic and continuous irradiation, is homogeneously and continuously stirred. In addition, the concentration of the excited state is assumed to be negligible, the medium temperature is constant, and at the (non–isosbestic) irradiation wavelength (λ_{irr}) species A and B absorb different amounts of light (P), i.e., the absorption coefficients (ε) of the species are different and have non-zero values ($\varepsilon_A^{\lambda_{irr}} \neq \varepsilon_B^{\lambda_{irr}} \neq 0$), is

$$\frac{dC_A\ (t)}{dt} = -\frac{dC_B\ (t)}{dt} = \left(\Phi_{B\to A}^{\lambda_{irr}} \times \varepsilon_B^{\lambda_{irr}} \times C_B\ (t) - \Phi_{A\to B}^{\lambda_{irr}} \times \varepsilon_A^{\lambda_{irr}} \times C_A\ (t)\right) \times l_{\lambda_{irr}} \times P_{\lambda_{irr}} \times F_{\lambda_{irr}}(t) \quad (1)$$

where $\Phi_{A\to B}^{\lambda_{irr}}$ and $\Phi_{B\to A}^{\lambda_{irr}}$ are the forward and reverse quantum yields of the photochemical steps realised at the irradiation wavelength (λ_{irr}), $P_{\lambda_{irr}}$ is the radiant power, $l_{\lambda_{irr}}$ is the optical path length of the irradiation beam inside the sample, and $F_{\lambda_{irr}}(t)$ the photokinetic factor expressed as:

$$F_{\lambda_{irr}}(t) = \frac{1 - 10^{-\left(A_{tot}^{\lambda_{irr}/\lambda_{irr}}(t) \times \frac{l_{\lambda_{irr}}}{l_{\lambda_{obs}}}\right)}}{A_{tot}^{\lambda_{irr}/\lambda_{irr}}(t) \times \frac{l_{\lambda_{irr}}}{l_{\lambda_{obs}}}} \quad (2)$$

Since $F_{\lambda_{irr}}(t)$ is a time-dependent function, Eq.1 has not been, thus far, integrated in a closed form. However, a semi–empirical integrated rate–law equation that describes the change of species concentration/absorbance as a function of time for AB(2Φ) systems has recently been proposed (Eq.3) (Maafi and Maafi, 2014).

$$A_{tot}^{\lambda_{irr}/\lambda_{obs}}(t) = A_{tot}^{\lambda_{irr}/\lambda_{obs}}(pss) + \frac{A_{tot}^{\lambda_{irr}/\lambda_{obs}}(0) - A_{tot}^{\lambda_{irr}/\lambda_{obs}}(pss)}{A_{tot}^{\lambda_{irr}/\lambda_{irr}}(0) - A_{tot}^{\lambda_{irr}/\lambda_{irr}}(pss)} \times \frac{l_{\lambda_{obs}}}{l_{\lambda_{irr}}}$$
$$\times Log\left[1 + \left(10^{\left[\left(A_{tot}^{\lambda_{irr}/\lambda_{irr}}(0) - A_{tot}^{\lambda_{irr}/\lambda_{irr}}(pss)\right) \times \frac{l_{\lambda_{irr}}}{l_{\lambda_{obs}}}\right]} - 1\right) \times e^{-k_{A \leftrightharpoons B}^{\lambda_{irr}} \times t}\right] \quad (3)$$

In this mathematical description, it is assumed that experimental measurements of spectroscopic ($A_{tot}^{\lambda_{irr}/\lambda_{obs}}$) and kinetic data are achieved under the observation ($l_{\lambda_{obs}}$) and not the excitation ($l_{\lambda_{irr}}$) conditions (with $l_{\lambda_{obs}}$ being the optical path length of the monitoring light inside the sample). It is important to notice that these optical path lengths ($l_{\lambda_{irr}}$ and $l_{\lambda_{obs}}$) are not necessarily equal, and the absorbance of the medium in the excitation conditions (i.e corresponding to a measurement along $l_{\lambda_{irr}}$) may not be directly accessible.

The coefficients $A_{tot}^{\lambda_{irr}/\lambda_{obs}}(t)$, $A_{tot}^{\lambda_{irr}/\lambda_{obs}}(0)$, $A_{tot}^{\lambda_{irr}/\lambda_{obs}}(pss)$, $A_{tot}^{\lambda_{irr}/\lambda_{irr}}(0)$ and $A_{tot}^{\lambda_{irr}/\lambda_{irr}}(pss)$ in Eq.3 are the measured (along $l_{\lambda_{obs}}$) total absorbances of the medium respectively recorded at reaction time t, at the initial time (t = 0) and at the photostationary state, *pss* (where t = ∞), when the reaction medium is irradiated at a given irradiation wavelength and simultaneously

monitored at either a different observation wavelength ($\lambda_{irr}/\lambda_{obs}$) or at the same wavelength ($\lambda_{irr}/\lambda_{irr}$). It is assumed that the reaction is quantitative and proceeds without by-products.

The analytical expression of the exponential factor, $k_{A\leftrightharpoons B}^{\lambda_{irr}}$, in Eq.3 which represents the overall reaction rate–constant, is given by (Maafi and Maafi, 2014).

$$k_{A\leftrightharpoons B}^{\lambda_{irr}} = \left(\Phi_{A\to B}^{\lambda_{irr}} \times \varepsilon_A^{\lambda_{irr}} + \Phi_{B\to A}^{\lambda_{irr}} \times \varepsilon_B^{\lambda_{irr}}\right) \times l_{\lambda_{irr}} \times P_{\lambda_{irr}} \times F^{\lambda_{irr}}(pss) \quad (4)$$

Where,

$$F^{\lambda_{irr}}(pss) = \frac{1 - 10^{-\left(A_{tot}^{\lambda_{irr}}(pss) \times \frac{l_{\lambda_{irr}}}{l_{\lambda_{obs}}}\right)}}{A_{tot}^{\lambda_{irr}}(pss) \times \frac{l_{\lambda_{irr}}}{l_{\lambda_{obs}}}} \quad (5)$$

Another derivation that can be extracted from Eq.1 is the initial velocity $\left((dA_{tot}/dt)_{t=0} = \upsilon_{0\,(cld.)}^{\lambda_{irr}/\lambda_{obs}}\right)$, for the kinetic trace involving the variation of the total absorbance (Maafi and Maafi, 2014),

$$\upsilon_{0\,(cld.)}^{\lambda_{irr}/\lambda_{obs}} = \left(\varepsilon_B^{\lambda_{obs}} - \varepsilon_A^{\lambda_{obs}}\right) \times l_{\lambda_{obs}} \times \Phi_{A\to B}^{\lambda_{irr}} \times \varepsilon_A^{\lambda_{irr}} \times l_{\lambda_{irr}} \times P_{\lambda_{irr}} \times F^{\lambda_{irr}}(0) \times C_0 \quad (6)$$

Which can also be obtained from the differentiation of Eq.3 (at t = 0), as (Maafi and Maafi, 2014)

$$\upsilon_{0\,(mod.)}^{\lambda_{irr}/\lambda_{obs}} = \left(\frac{dA_{tot}^{\lambda_{irr}/\lambda_{obs}}}{dt}\right)_0 =$$

$$\frac{A_{tot}^{\lambda_{irr}/\lambda_{obs}}(0) - A_{tot}^{\lambda_{irr}/\lambda_{obs}}(pss)}{A_{tot}^{\lambda_{irr}/\lambda_{irr}}(0) - A_{tot}^{\lambda_{irr}/\lambda_{irr}}(pss)} \times \frac{k_{A \leftrightharpoons B\,(mod.)}^{\lambda_{irr}}}{\frac{l_{\lambda_{irr}}}{l_{\lambda_{obs}}} \times Ln(10)} \times \left(10^{\left(A_{tot}^{\lambda_{irr}/\lambda_{irr}}(pss) - A_{tot}^{\lambda_{irr}/\lambda_{irr}}(0)\right) \times \frac{l_{\lambda_{irr}}}{l_{\lambda_{obs}}}} - 1\right) \qquad (7)$$

3.2. Monte photoreaction and Φ–order kinetics

Monte is highly photo–unstable especially in solution (Roman et al, 2011; Alsarra, 2004; Al Omari et al, 1999) even when exposed to very low UV–energy levels (Roman et al, 2011; Alsarra, 2004; Al Omari et al, 1999) (Scheme 1).

The electronic absorption spectrum of Monte is characterised by an intense peak at *ca.* 210 nm and a second broad and vibrational transition band spanning the 250 – 400 nm region. The spectral evolution of the solution when exposed to a continuous monochromatic irradiation (Fig.1) shows an increase and a decrease of the absorbances in the wavelength regions respectively above (200-258 nm) and below (258-400 nm) the isosbestic point (λ_{isos} = 258 nm). This indicates that *trans*– and *cis*–Monte isomers share the same overall shape of the absorption spectra (they totally overlap and no new features appear, during

219 photodegradadtion, on the original spectrum). These findings also suggest that the reaction is
220 quantitative and proceeds without by–products.

221

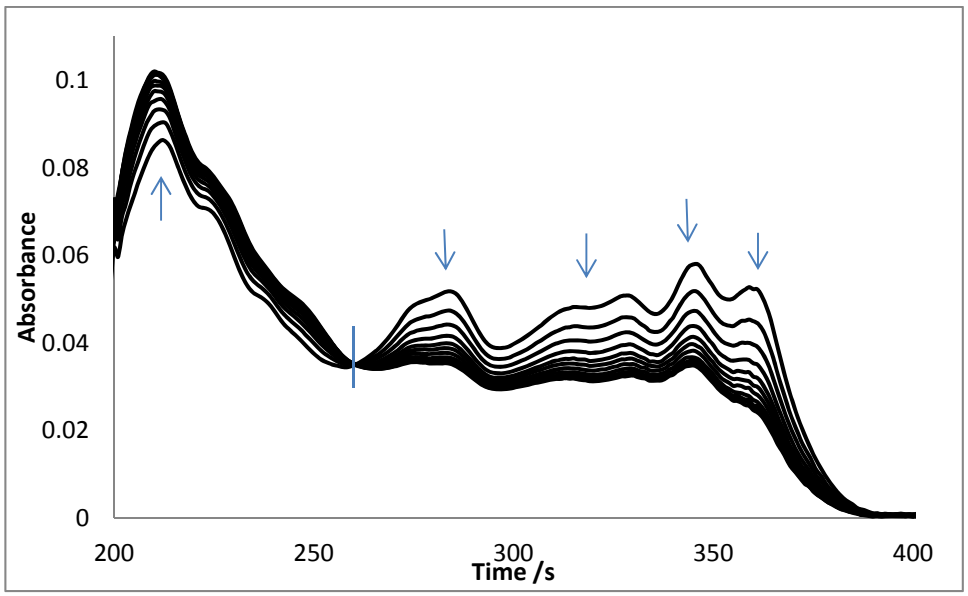

222

223 **Fig. 1.** Evolution of the electronic absorption spectra of 1.85 x 10^{-6} M Monte in ethanol
224 subjected to a continuous irradiation with a 360-nm monochromatic beam (total irradiation
225 time 700 s at a radiant power of P_{360} = 9.86 x 10^{-7} einstein.s^{-1}.dm^{-3}). The arrows indicate the
226 direction of the peaks' evolution during the photoreaction and the vertical line crosses the
227 spectra at the isosbestic point.

228

229 Monte ethanolic solutions were also studied under various irradiations spanning Monte
230 absorption spectrum at 220, 258, 284, 328, 345 and 360 nm. In each case, the kinetic trace of
231 the degradation was recorded at an observation wavelength of 345 nm (Fig.2). As can be seen,
232 the traces follow a smooth decrease, eventually reaching a plateau region. This behaviour
233 corroborates the AB(2Φ) mechanism proposed for Monte (Scheme 1).

234

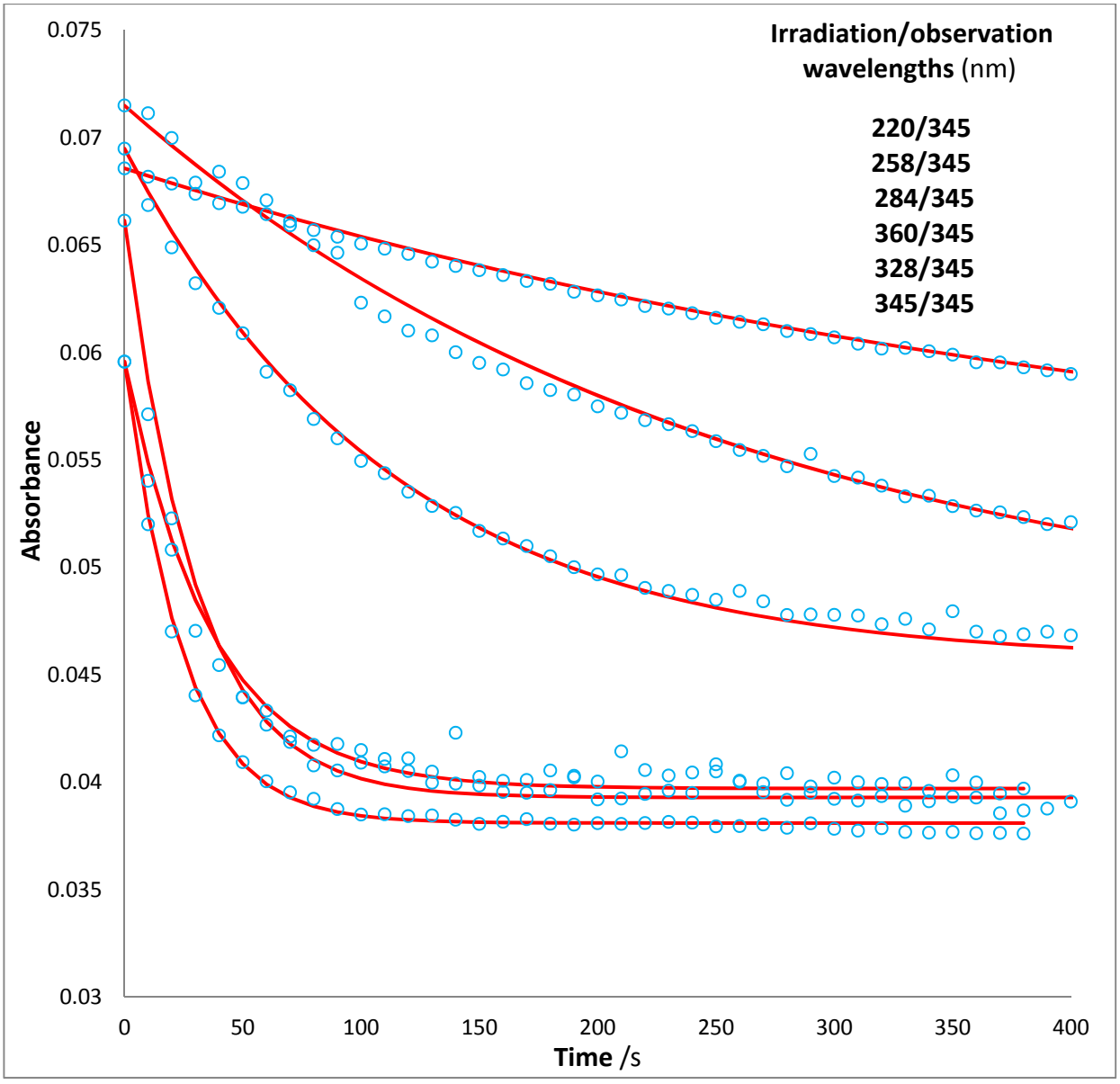

Fig. 2. Photokinetic traces of Monte in ethanol (1.85 x 10^{-6} M) at λ_{irr}= 220, 258, 284, 360, 328 and 345 nm and observed at λ_{obs} = 345nm. The circles represent the experimental data while the lines represent the fitting traces using Eq.3.

The experimental traces were all well fitted by Eq.3 (Fig.2), indicating that the developed model describes faithfully the kinetics of Monte photodegradation. This also clearly indicates that Monte obeys Φ–order kinetics.

The overall rate–constants ($k_{A\leftrightharpoons B}^{\lambda_{irr}} = k_{Trans\leftrightharpoons Cis}^{\lambda_{irr}}$) obtained from the fitting of the traces (Table 1), seem to increased with wavelength (Table 1). Nonetheless, the $k_{Trans\leftrightharpoons Cis}^{\lambda_{irr}}$ values must be considered with caution because they cannot be directly compared for the present experiments (Fig.2), since they depend on both spectral, reactivity and experimental conditions (as clearly stated in Eq.4). The quantity$\left(\Phi_{A\to B}^{\lambda_{irr}} \times \varepsilon_A^{\lambda_{irr}} + \Phi_{B\to A}^{\lambda_{irr}} \times \varepsilon_B^{\lambda_{irr}}\right)$, worked out from the expression of $k_{A\leftrightharpoons B}^{\lambda_{irr}}$ and the experimental parameters, would not be a better criterion for comparing the effects of irradiation wavelengths since both quantum yields and absorption coefficients, involved in the expression of the above quantity, may be wavelength–dependent. This argument raises a much wider point about the usefulness of the experimentally determined AB(2Φ) reactions' overall rate–constants especially when polychromatic light and/or first–order kinetics are employed. Hence, it is mandatory to elucidate the kinetics in order to determine all the parameters of the reactions including the quantum yield values of the individual photochemical steps.

Table 1

Overall photoreaction rate-constants, spectroscopic and kinetic parameter values of Monte for a set of monochromatic irradiations performed in ethanol at 22°C.

λ_{irr} /nm	$A_{tot}^{\lambda_{irr}/345}(0)$	$P_{\lambda_{irr}}$ /einstein. s^{-1}. dm^{-3}	$A_{tot}^{\lambda irr/\lambda irr}(pss)$	$k_{A\leftrightharpoons B}^{\lambda_{irr}}$ /s^{-1}	$\Phi_{A\to B}^{\lambda_{irr}} \times \varepsilon_A^{\lambda_{irr}} + \Phi_{B\to A}^{\lambda_{irr}} \times \varepsilon_B^{\lambda_{irr}}$ /L. mol^{-1}. cm^{-3}
220	0.068	8.009 x 10^{-7}	0.088	0.0021	692
258	0.071	6.362 x 10^{-7}	0.044	0.0039	1472
284	0.069	6.932 x 10^{-7}	0.043	0.0092	3183
328	0.060	1.187 x 10^{-6}	0.033	0.028	5523
345	0.060	1.428 x 10^{-6}	0.038	0.042	6958
360	0.066	1.332 x 10^{-6}	0.026	0.035	6058

3.3. *Kinetic elucidation method*

The elucidation of Monte kinetics amounts to the determination of the three unknown reaction attributes, namely the forward ($\Phi_{A\to B}^{\lambda}$) and the reverse ($\Phi_{B\to A}^{\lambda}$) quantum yields, and the spectrum of the photoproduct (ε_B^{λ} of *cis*–Monte isomer). These parameters will not be worked out from the kinetic traces alone because the useful equations (mainly Eqs. 4, 6 and that of $A_{tot}(pss)$) cannot be solved for the three aforementioned parameters due to the fact that these equations, even though linearly-independent, are non-linear. This situation represents a typical example of an unidentifiability problem as has previously been discussed for a few kinetic cases (Maafi and Brown, 2008; Maafi and Brown, 2005b). The identifiability problem is due to the great flexibility that is inherent to the system of non-linear equations which leads to a degenerate solution, i.e., usually a large number of sets of values can be found for the three unknown parameters ($\Phi_{A\to B}^{\lambda_{irr}}$, $\Phi_{B\to A}^{\lambda_{irr}}$ and $\varepsilon_B^{\lambda_{irr}}$). In Eq.3, each of these sets (of three parameters) would provide data that equally fit the experimental traces with high accuracy so that the one that represents the true kinetic solution cannot be identified. As a matter of fact, the knowledge of the integrated rate-law (Eq.3) of the photodegradation reaction is important to characterise the unidentifiability problem (if any exist) but it is insufficient to achieve a comprehensive elucidation of the kinetics.

Accordingly, further data (obtained by alternative analytical means) are required to perform the elucidation. The new AB(2Φ)-kinetic elucidation method, presented for the first time in this study for Monte photodegradation, will be realised in three stages.

Firstly, the photodegradation reaction subjected to a monochromatic irradiation at the isosbestic point is monitored by HPLC. At this irradiation wavelength (λ_{isos}), the absorption coefficient of cis-Monte is known ($\varepsilon_A^{\lambda_{isos}} = \varepsilon_B^{\lambda_{isos}}$). The HPLC allows obtaining the variation of the concentrations of the species involved in the reaction and not the absorbances. This means that the number of unknowns is only two for this experiment.

In a second step, the fitting of the concentration curves obtained by HPLC allows the determination of the numerical values for the reaction initial velocity ($v_0^{\lambda_{isos}}$) and the reaction rate-constant ($k_{A\leftrightharpoons B}^{\lambda_{isos}}$). Because the data correspond to a reaction realised under isosbestic irradiation, the latter parameters depend on only two unknowns ($\Phi_{A\to B}^{\lambda_{isos}}$ and $\Phi_{B\to A}^{\lambda_{isos}}$). Therefore, the absolute values of $\Phi_{A\to B}^{\lambda_{isos}}$ and $\Phi_{B\to A}^{\lambda_{isos}}$ are easily worked out from the equations of $v_0^{\lambda_{isos}}$ and $k_{A\leftrightharpoons B}^{\lambda_{isos}}$.

Knowing the values of these parameters facilitates, in a third step, the reconstruction of the full spectrum of the photoisomer (cis-Monte).

Finally, by knowing the spectrum of the photoproduct (ε_B^{λ}) the number of unknowns will constantly be two irrespective of the irradiation wavelength selected. Hence, the quantum yields for such irradiation condition ($\Phi_{A\to B}^{\lambda_{irr}}$ and $\Phi_{B\to A}^{\lambda_{irr}}$) can readily be worked out.

The detailed application of these steps to Monte reaction is presented hereafter.

The quantum yields of the photochemical reaction steps at an isosbestic wavelength can be extracted from the traces of the isomers obtained by monitoring the variation of the isomers concentrations by HPLC. When the monochromatic irradiation of the solution is realised at an isosbetic point ($\lambda_{irr} = \lambda_{isos}$) the reaction traces obey first–order kinetics according to the integrated rate-law expressions (Eqs. 8 and 9) (Maafi and Brown, 2005a).

$$C_A(t) = C_A(pss) + \left(C_A(0) - C_A(pss)\right) \times e^{-k_{A \leftrightharpoons B}^{\lambda_{isos}} \times t} \quad (8)$$

$$C_B(t) = C_B(pss) - C_B(pss) \times e^{-k_{A \leftrightharpoons B}^{\lambda_{isos}} \times t} \quad (9)$$

where $C_A(pss)$ and $C_B(pss)$ are the concentrations of the species at *pss* and $k_{A \leftrightharpoons B}^{\lambda_{isos}}$ the overall rate-constant of the reaction performed at an isosbetic irradiation.

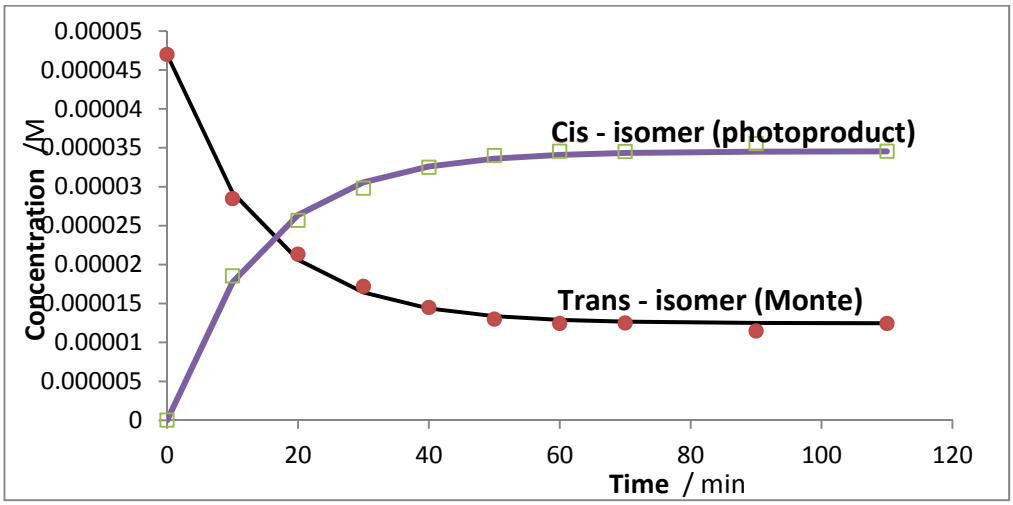

Fig. 3. Evolution of Monte concentration over photodegradation time and formation of the *cis*–isomer photoproduct monitored by HPLC upon exposure to isosbestic monochromatic irradiation of 258 nm (P_{258}= 6.43 x 10^{-7} einstein.s^{-1}.dm^{-3}).

These model equations fit well the experimental data (Fig.3) and allow the determination of both the initial velocity ($v_0^{\lambda_{isos}}$, whose formulae are worked out from Eqs.1 and 8), and the overall reaction rate-constant ($k_{A\leftrightharpoons B}^{\lambda_{isos}}$), as

$$v_0^{\lambda_{isos}} = -k_{A\leftrightharpoons B}^{\lambda_{isos}} \times \left(C_A(0) - C_A(pss)\right) = -\Phi_{A\to B}^{\lambda_{isos}} \times C_A(0) \times \varepsilon_A^{\lambda_{isos}} \times l_{\lambda_{isos}} \times P_{\lambda_{isos}} \times F_{\lambda_{isos}} \quad (10)$$

$$k_{A\leftrightharpoons B}^{\lambda_{isos}} = \left(\Phi_{A\to B}^{\lambda_{isos}} + \Phi_{B\to A}^{\lambda_{isos}}\right) \varepsilon_A^{\lambda_{isos}} \times l_{\lambda_{isos}} \times P_{\lambda_{isos}} \times F_{\lambda_{isos}} \quad (11)$$

with the terms of these equations have the same meaning as before except that they are expressed relative to the isosbetic irradiation (λ_{isos}). $F_{\lambda_{isos}}$ was calculated by replacing $A_{tot}^{\lambda_{irr}/\lambda_{irr}}(t)$ with $A_{tot}^{\lambda_{isos}}$ in Eq.2.

The absolute value of the forward quantum yield ($\Phi_{A\to B}^{\lambda_{isos}}$) can readily be worked out from Eq.10. The latter values in combination with Eq.11 leads to the determination of the value of the reverse quantum yield at the isosbestic point ($\Phi_{B\to A}^{\lambda_{isos}}$). As a result, the equilibrium constant, $\mathrm{K}_{\leftrightharpoons}^{\lambda_{isos}}$, expressed as the ratio of the species concentrations at *pss* for the isosbestic irradiation, given by Eq.12 can be calculated.

$$\mathrm{K}_{\leftrightharpoons}^{\lambda_{isos}} = \frac{k_{B\to A}^{\lambda_{isos}}}{k_{A\to B}^{\lambda_{isos}}} = \frac{C_B(pss)}{C_A(pss)} = \frac{\Phi_{A\to B}^{\lambda_{isos}}}{\Phi_{B\to A}^{\lambda_{isos}}} \quad (12)$$

The results shown in Table 2 indicate that the *trans*–Monte isomer is much more photoreactive than its counterpart as the ratio of their quantum yields at the *pss* is greater than unity ($\mathrm{K}_{\leftrightharpoons}^{\lambda_{isos}} = 2.75$).

Table 2

Quantum yields, $\mathrm{K}_{\leftrightharpoons}^{\lambda_{isos}}$ and overall rate-constant values for the photodegradation of Monte under isosbestic monochromatic irradiation conditions.

$\boldsymbol{\lambda_{isos}}$ /nm	$\boldsymbol{A_0^{\lambda_{isos}}}$	$\boldsymbol{C_A}(0)$ / M	$\boldsymbol{l_{\lambda_{isos}}}$ / cm	$\boldsymbol{l_{\lambda_{obs}}}$ / cm	$\boldsymbol{C_A(pss)}$ / M	$\boldsymbol{C_B(pss)}$ / M	$\boldsymbol{P_{\lambda_{isos}}}$ /einstein.s^{-1}.dm^{-3}	$\boldsymbol{F_{\lambda_{isos}}}$	$\boldsymbol{k_{A\leftrightharpoons B}^{\lambda_{isos}}}$ / s^{-1}	$\boldsymbol{\Phi_{A\to B}^{\lambda_{isos}}}$	$\boldsymbol{\Phi_{B\to A}^{\lambda_{isos}}}$	$\mathrm{K}_{\leftrightharpoons}^{\lambda_{isos}}$
258	0.92	4.7x10^{-5}	2	1	1.24 x10^{-5}	3.45x10^{-5}	6.43x10^{-7}	0.53	1.17x10^{-3}	0.066	0.024	2.75

The reconstruction of the whole spectrum of the *cis*–isomer is obtained (Fig.4) from the spectrum of the reactive medium at *pss* when subjected to an isosbestic irradiation ($A_{tot}^{\lambda_{isos}/\lambda_{obs}}(pss)$) and the value of the concentration-independent parameter, $\mathrm{K}_{\leftrightharpoons}^{\lambda_{isos}}$ (Table 1), as

$$\varepsilon_B^{\lambda_{obs}} = \frac{(\mathrm{K}_{\leftrightharpoons}^{\lambda_{isos}} + 1) \times A_{tot}^{\lambda_{isos}/\lambda_{obs}}(pss) - \varepsilon_A^{\lambda_{obs}} \times l_{obs} \times C_A(0)}{l_{obs} \times \mathrm{K}_{\leftrightharpoons}^{\lambda_{isos}} \times C_A(0)} \qquad (13)$$

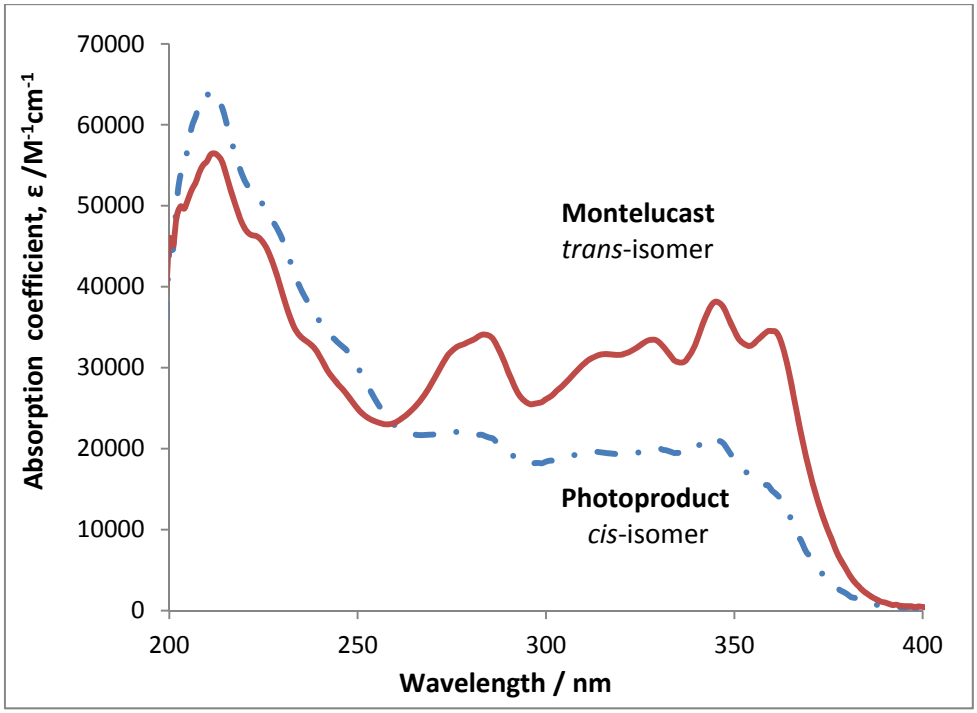

354

355 **Fig. 4.** Native and reconstructed electronic absorption spectra (absorption coefficient units) of
356 Monte and its *cis*–isomer photoproduct, respectively.

357

358 Once the absorption coefficients of the *cis*–isomer are known, the photochemical quantum yields of
359 *trans*– and *cis*–Monte isomers can be determined at any irradiation wavelength (Table 3), in the
360 final step of the method, by using a combination of Eqs. 4, 6 and 7.

361

362 A 15-fold increase is recorded for the forward quantum yield values in the wavelengths interval
363 situated between 220nm and 360nm (Table 3). This confirms that the UVA is the photodegradation
364 causative irradiation for Monte. The linear plot obtained for the correlation of the forward quantum
365 yield against irradiation wavelength (Fig.5), facilitates the calculated of quantum yield values at any
366 wavelength in the range 220 – 360 nm.

367

Table 3

Quantum yields, overall rate-constant, absorption coefficient and initial velocity values for Monte photodegradation reactions under various monochromatic irradiations.

λ_{irr} /nm	$P_{\lambda_{irr}}$ /einstein. $s^{-1}.dm^{-3}$	$A_{tot}^{\lambda_{irr}/345}(pss)$	$k_{A\leftrightarrows B}^{\lambda_{irr}}$ /s^{-1}	$\upsilon_0^{\lambda_{irr}/\lambda_{obs}}$ / s^{-1}	$\varepsilon_{Trans}^{\lambda_{irr}}$ / $M^{-1}cm^{-1}$	$\varepsilon_{Cis}^{\lambda_{irr}}$ / $M^{-1}cm^{-1}$	$F_{\lambda_{irr}}(0)$	$\Phi_{A\to B}^{\lambda_{irr}}$	$\Phi_{B\to A}^{\lambda_{irr}}$
220	**8.009×10^{-7}**	**0.088**	**0.0021**	**-3.51×10^{-5}**	**47235**	**53121**	**1.910**	**0.012 ± 0.0011**	**0.0033 ± 0.0004**
258	**6.362×10^{-7}**	**0.044**	**0.0039**	**-7.2×10^{-5}**	**23003**	**23762**	**1.999**	**0.065 ± 0.0007**	**0.024 ± 0.0057**
284	**6.932×10^{-7}**	**0.044**	**0.0092**	**-0.00021**	**34076**	**21517**	**1.999**	**0.072 ± 0.0046**	**0.039 ± 0.0063**
328	**1.187×10^{-6}**	**0.033**	**0.028**	**-0.00054**	**33446**	**19988**	**2.055**	**0.145 ± 0.0121**	**0.061 ± 0.0282**
345	**1.428×10^{-6}**	**0.038**	**0.042**	**-0.00086**	**38149**	**21345**	**2.014**	**0.160 ± 0.0125**	**0.060 ± 0.0034**
360	**1.332×10^{-6}**	**0.026**	**0.035**	**-0.0009**	**34519**	**14823**	**2.003**	**0.180 ± 0.0129**	**0.021 ± 0.0068**

The reverse quantum values were found between 12 to 54 % smaller than those of $\Phi_{A\to B}^{\lambda_{irr}}$ throughout the spectral range studied (Table 3). Their evolution with wavelength has however an overall concave shape (Fig.5), indicating that the *cis*–isomer is mostly photochemically active in the wavelength region situated between 280 and 350 nm (beyond that region, $\Phi_{B\to A}^{\lambda_{irr}} < 0.025$). The disparity in the wavelength-dependence of the quantum yields might suggest a different excited–state for each isomer. This might agree with Kasha's rule prediction, as the ratio of quantum yields of *cis*–trans isomers would be mostly wavelength–invariant if the two species shared a common excited–state.

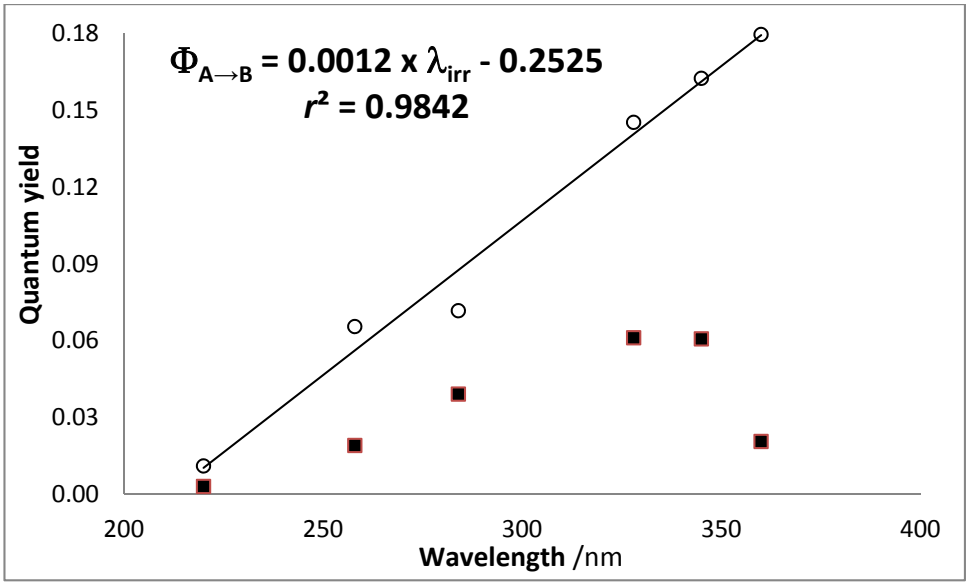

381

382 **Fig. 5.** Average forward ($\Phi_{A\rightarrow B}^{\lambda_{irr}}$) (circles) and reverse ($\Phi_{B\rightarrow A}^{\lambda_{irr}}$) (plain squares) quantum yields
383 calculated for irradiation wavelengths 220, 258, 285, 328, 345 and 360 nm.
384 Inset: the linear– relationship equation of the forward quantum yield with irradiation wavelength.

385

386

387 The present kinetic study offers a novel approach to elucidate the kinetics of AB(2Φ)
388 photoreversible systems, which can fill a gap in photokinetic and drug photodegradation
389 studies. Thus far, the photodegradation of Monte, generally studied in organic media by
390 monitoring the variation of its concentration by HPLC, has usually led to assign first-order
391 kinetics to the reaction based on a good linear plot (Al Omari et al., 2007; Alsarra, 2004). The
392 authors however did not investigate further whether the data could be fitted with equations
393 corresponding to other reaction-orders.

394

395 More recently, a different approach was proposed (Roman et al., 2011). The kinetic order of
396 Monte photodegradation was only ascribed after generating three plots, assuming that the
397 reaction obeyed 0^{th}–, 1^{st}– and 2^{nd}–orders, respectively, and then a decision about reaction–

order attribution was reached by evaluating the correlation coefficients of the plots. Accordingly, the study attributed a zero–order for Monte photodegradation as the linear kinetic data for this case were characterised by the highest correlation coefficient (r^2 = 0.996), despite the fact that the two other correlations were satisfactory (r^2 values of 0.9937 and 0.9723, respectively for first- and second-order kinetics).

From a general point of view, Monte is not an isolated case where the order of the drug photoreaction is either pre–assumed or defined on the basis of a good fit (Piechocki and Thoma, 2010). Sometimes it is difficult to reach a decision about the order of the studied reaction as a good fit may well be obtained for the reaction's kinetic data when they have been analysed according to different reaction–order options. The cases of benzydamine hydrochloride and ketrolac thromethamine (Piechocki and Thoma, 2010) represent another good example of such ambiguities since each of the datasets fitted well both zero– and first–order kinetics.

A high correlation coefficient is obviously not sufficient to validate such approaches as it is a matter of fact, that the formulae set out for 0^{th}–, 1^{st}– and 2^{nd}–order reactions, originally developed for pure thermal reactions, can only be justified for photoreactions performed under isosbestic irradiations (such as Eqs.8 and 9) but certainly not for non-isosbestic irradiations, as proved in the present and previous studies (Maafi and Maafi, 2013), and/or when polychromatic light is used (as it is ubiquitously employed in the literature). In addition, the reaction overall rate–constant values obtained from such strategies or even through a strategy based on Φ–order kinetics should not be considered as conveying a reliable

quantification of the reaction progress in different situations, as $k^{\lambda}_{A \leftrightharpoons B}$ depends on various intrinsic factors to the drug, the photoproduct, as well as on experimental conditions (Eq.4). This reiterates the importance of determining the absolute values of the quantum yields of all the species involved in the reaction. The elucidation method presented in this study solves the issue for photoreversible reactions, nonetheless, more effort should be conceded to develop similar strategies for more extended mechanisms of drugs' photodegradations.

In this respect, it is also worth mentioning that our approach is the first kinetic–based method for the determination of the absolute values for AB(2Φ) species quantum yields. This might prove to be a better alternative to the methods proposed in the literature. Indeed, it is usually the case that the quantum yield of a given reaction is calculated by dividing the number of molecules of the initial drug–species that had reacted (most often obtained by chromatography), by the number of photons or the radiant power determined for the light–source (Ricci et al, 2003; Ricci et al 2001). The validity of such a method raises some important questions since not only the initial drug–molecule but also its photoproducts and the products thermally- or photochemically–generated from the photoproducts themselves, may significantly contribute to the absorption of the incident photons of the light–source. Therefore the actual number of photons absorbed by the initial drug–molecule is less than the radiant power received by the sample. It is also important to mention that this method yields a unique (average) quantum yield value for the whole reaction, assumed to be subjected to a monochromatic excitation beam, as it is not capable of distinguishing the individual (additional) photoreactions that may be involved in the overall photodegradation process (crucially, when the initial species is depleted via a divergent reaction and/or regenerated during the reaction

444 course as for a photoreversible reaction). It is also worth noting that the quantum yield values
445 obtained in this manner can only be considered reliable if the reaction investigated is a pure
446 unimolecular, AB(1Φ), photoreaction for which the photoproduct does not absorb the incident
447 irradiation light (our previous results on AB(1Φ) nifedipine kinetics have shown a variation of
448 the reaction behaviour when nifedipine absorbs alone and when both nifedipine and its
449 photoproduct absorb (Maafi and Maafi, 2013)).

450

451 Therefore, kinetic methods as the one proposed here, represent a more reliable alternative for
452 the determination of the quantum yields of photoreactive systems, as the integrated rate–laws
453 and the overall rate–constant equations implicitly take into account not only the various
454 individual photochemical reaction–steps but also and more importantly the absorption
455 contribution of the various species involved.

456

457

458 3.4. *Development of a Monte-based actinometric method*

459

460 Each freshly-made Monte solution was subjected to an irradiation beam of varying radiant
461 power for a set of four UVA wavelengths (258, 328, 345 and 360 nm), spanning the whole
462 second electronic absorption band of Monte (whose transition bands are mainly responsible
463 for Monte photoreactivity). The experimental traces, obtained for the *j* radiant power values at
464 a given λ_{irr} were fitted with the Φ–order model (Eq.3 and Fig.6).

465

A good fitting was observed for the acquired experimental traces (Fig.6), further confirming that Monte obeys Φ–order kinetics. As expected, the reactions were found to occur faster with increasing radiant power, in agreement with the formulation of the overall rate-constant equation (Eq.14).

$$k_{A\leftrightharpoons B}^{\lambda_{irr}} = \left(\Phi_{A\to B}^{\lambda_{irr}} \times \varepsilon_A^{\lambda_{irr}} + \Phi_{B\to A}^{\lambda_{irr}} \times \varepsilon_B^{\lambda_{irr}}\right) \times l_{\lambda_{irr}} \times P_{\lambda_{irr}} \times F_{\lambda_{irr}}(pss) = \beta_{\lambda_{irr}} \times P_{\lambda_{irr}} \quad (14)$$

Therefore, plots of $k_{A\leftrightharpoons B}^{\lambda_{irr}}$ against $P_{\lambda_{irr}}$ for each wavelength experiment yielded a straight line with correlation coefficients values over 0.98 and intercepts very close to zero (Table 4). The gradient of the linear relationship, the factor $\beta_{\lambda_{irr}}$ (E.15), is constant for a given irradiation wavelength, as given by the formula

$$\beta_{\lambda_{irr}} = \left(\Phi_{A\to B}^{\lambda_{irr}} \times \varepsilon_A^{\lambda_{irr}} + \Phi_{B\to A}^{\lambda_{irr}} \times \varepsilon_B^{\lambda_{irr}}\right) \times l_{\lambda_{irr}} \times F_{\lambda_{irr}}(pss) \quad (15)$$

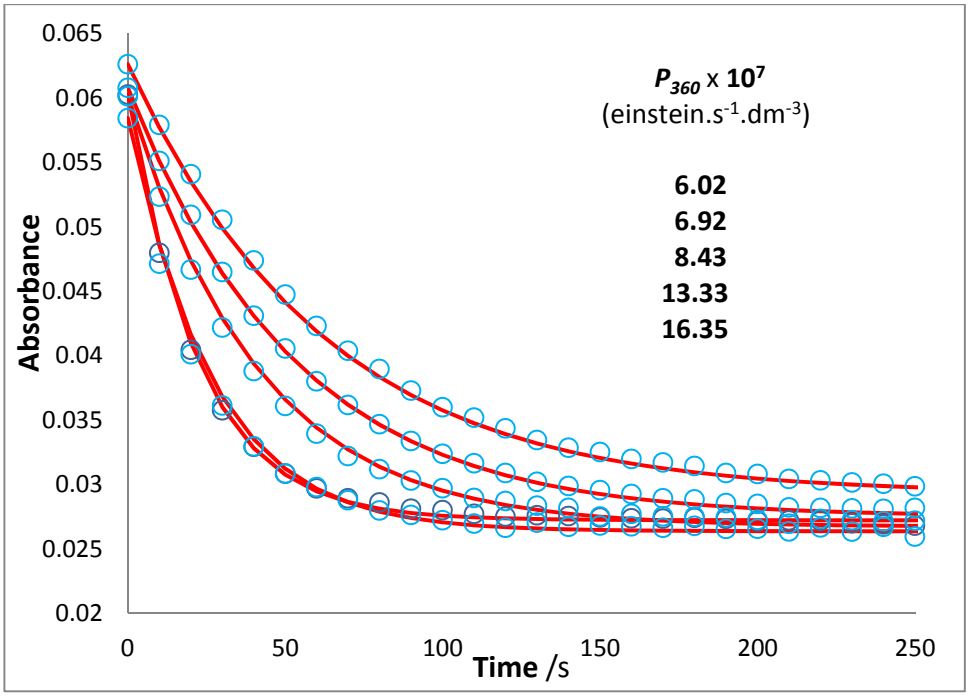

Fig. 6. Effect of increasing the radiant power of the monochromatic irradiation beam on the kinetic traces of Monte (1.85 x 10^{-6} M) when irradiated and observed at 360 nm. The circles represent the experimental data and the lines, the traces obtained from the model equation.

Table 4

Correlation equations for the variation of Monte photodegradation overall rate-constants ($k_{A\leftrightharpoons B}^{\lambda_{irr}}$) with radiant power ($P_{\lambda_{irr}}$), the corresponding $\beta_{\lambda_{irr}}$ factor values, and the span of radiant power employed for various monochromatic irradiations.

Irradiation wavelength λ_{irr} / nm	**Equation of the line** [a] $k_{A\leftrightharpoons B}^{\lambda_{irr}} = \beta_{\lambda_{irr}} \times P_{\lambda_{irr}} + intercept$	**Correlation coefficient, r^2**	**$P_{\lambda_{irr}} \times 10^7$ einst.s^{-1}.dm^{-3}**
360	$28069 \times P_{360} + 8 \times 10^{-4}$	0.9957	6.02 – 16.3
345	$24932 \times P_{345} + 4 \times 10^{-3}$	0.9803	4.99 – 14.1
328	$17064 \times P_{328} + 7.9 \times 10^{-3}$	0.9994	5.67 – 13.1
258	$2250.7 \times P_{258} + 1.1 \times 10^{-3}$	0.9839	4.53 – 10.0

[a] $k_{A\leftrightharpoons B}^{\lambda_{irr}}$ and intercepts expressed in s^{-1} and $\beta_{\lambda_{irr}}$ in einst^{-1}.dm^3

It is interesting to notice that for Monte, the factor $\beta_{\lambda_{irr}}$ is relatively well correlated to the irradiation wavelength by a linear relationship (Fig. 7). This allows the determination of the $\beta_{\lambda_{irr}}$ factors at any wavelength within the selected range (258 – 360 nm), and helps the development of an actinometric method.

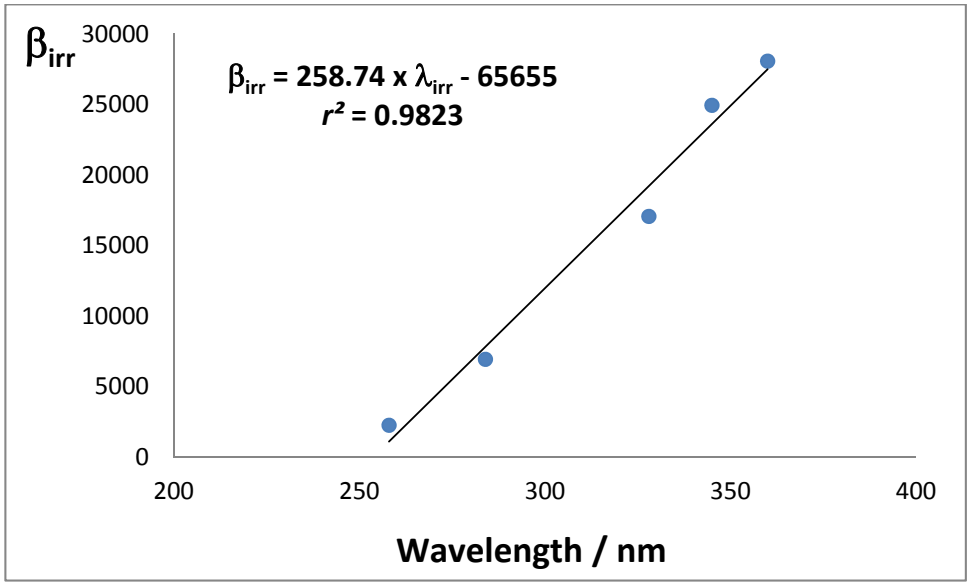

Fig. 7. Linear correlation of $\beta_{\lambda_{irr}}$ (Table 4) with irradiation wavelength. $\beta_{\lambda_{irr}}$ is expressed in einst^{-1}.dm^{3}.

Even though the determination of the $\beta_{\lambda_{irr}}$ factors does not require a prior knowledge of the reaction attributes, there is however a good correlation between the experimental values of $\beta_{\lambda_{irr}}^{exp.}$ factors determined by actinometry (Table 4) and those calculated ($\beta_{\lambda_{irr}}^{cld.}$) using both Eq.15 and the data of Table 3, as shown in Fig.8.

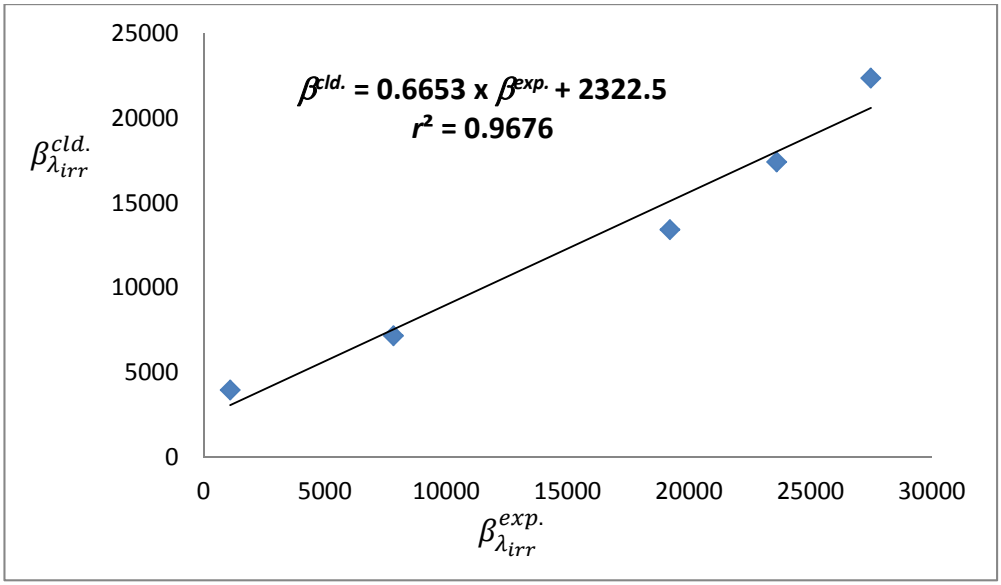

509

510 **Fig. 8.** Correlation between calculated and experimental, respectively, $\beta_{\lambda_{irr}}^{cld.}$ and $\beta_{\lambda_{irr}}^{exp.}$ factors.

511

512 The following actinometric method could be used for Monte's full absorption spectrum. Its
513 implementation can be performed in stages. In order to measure the radiant power of an
514 unknown light-source, a monochromatic irradiation is performed on a freshly-made Monte
515 ethanolic solution (*c.a.* 2 x 10^{-6} M), at a selected wavelength (between 258 and 360 nm). The
516 experimental trace hence obtained for Monte phototransformation is fitted to the Φ–order
517 model equation (Eq.3) and the reaction overall rate-constant value determined. Subsequently,
518 the actual radiant power of the source can be readily calculated using the simple formula
519 (Eq.16) comprising the values of the measured overall rate-constant for Monte
520 photodegradation, and the selected irradiation wavelength, as

521

$$P_{\lambda_{irr}} = \frac{k_{A \leftrightarrows B}^{\lambda_{irr}}}{258.74 \times \lambda_{irr} - 65655} \qquad (16)$$

522 Furthermore, the procedure is readily applicable to high radiant power light-sources (as proved
523 by the RK-simulated results (Maafi and Maafi, 2014)) that can be necessary to study the
524 absorption wavelength sections where the reaction is characterised by weak efficiencies as for
525 λ_{irr} < 250 nm in the case of Monte.

526

527 It is also important to underline that the actinometric strategies developed in our studies are
528 complementary as UVB, UVA and visible ranges, spanning the 300 nm-wide, 260 – 570 nm,
529 spectral region, can be readily covered by Monte, nifedipine and a diaryethene actinomters
530 (Maafi and Maafi, 2013; Maafi, 2010). In addition, these approaches are certainly not limited to
531 the aforementioned species but can easily be extended to many other photo-drugs obeying
532 similar types of mechanisms (i.e. unimolecular or photoreversible reactions).

533

534 The straightforward actinometric method proposed in this work can be considered as a good
535 alternative to the existing approaches, especially for the ICH recommended procedure
536 employing quinine hydrochloride as a chemical actinometer (ICH, 1996), whose drawbacks and
537 limitations have been reviewed in a number of reports (Baertschi, 1997; Baertschi et al., 2009,
538 2010, De Azevedo Filho et al., 2011; Kester et al., 1996; Maafi and Maafi, 2013; Piechocki and
539 Thoma, 2010; Tonnesen, 2004).

540

541 Methods for polychromatic-light actinometry that would be based on kinetic treatments need
542 yet to be developed. Nonetheless, it might turn out that monochromatic actinometry is the
543 way forward for the development of such polychromatic actinometric methods as the latter

suffer not only from a lack of a comprehensive mathematical background to describe such complex multi-absorption processes, but also because the number of photons absorbed by the actinometer may not necessarily be the same specific number of photons absorbed by the reactive molecule or drug under investigation. This would be the case whenever the actinometer species and the investigated photodegradable drug have different absorption spectra and/or different absorption coefficients within the spectral regions of interest. In this respect, it is also important to stress that a polychromatic actinometer might need to be recalibrated for each new light-source and at different stages of the lamp's life-time as irradiance profiles are both source-specific and time-evolving.

4. Conclusion

The photokinetic traces of Monte are well described by the newly proposed integrated AB(2Φ) rate-model (Eq.3) indicating that the reaction, subjected to non-isosbestic irradiation, obeys Φ–order kinetic. These and previous results (Maafi and Maafi, 2013) strongly suggest that photodegradation reactions of drugs are better ascribed a Φ–order rather than the usually predicted but controversial thermal reaction orders.

The stepwise approach proposed here to elucidate Monte photokinetics is, as a matter of fact, a general approach for any AB(2Φ) drug or system. It is readily capable of solving the identifiability issues inherent to such non-linear systems. It, henceforward, allows the determination of the quantum yields at individual irradiation wavelengths. Consistent with the fact that the quantum yields of drug photodegradations must, *a priori*, be considered wavelength-dependent, the measurement of an average value for the cases studied in the literature where a polychromatic irradiation is performed, might result in misleading conclusions and should be considered with caution. For Monte, up to a 15-fold increase was recorded for its forward quantum yield value between 220 and 360 nm. However, the variation of its reverse quantum yield values within the same irradiation wavelength range was concave, with an 18–fold maximum span of variation, calculated as the ratio of highest to lowest $\Phi_{B\rightarrow A}^{\lambda_{irr}}$ values.

578 An interesting advantage of the mathematical formulation proposed for the Φ–order reactions
579 is its flexibility to model other relevant parameters. It has successfully been applied to prove
580 the usefulness in developing new drug-actinometers such as Monte in the 260 – 360 nm
581 dynamic range. Not only the actinometric-kinetic method proposed here for the first time is
582 simple to implement, reliable and cost-effective, but also the results found for Monte can be
583 combined with those obtained for other drugs and systems in order to propose a poly–
584 actinometer system able to cover the largest possible spectral region. Thus far, the Monte-
585 Nifedipine-DAE actinometer, spanning the 260 – 570 nm spectral range, might be considered as
586 an alternative to the ICH proposed quinine hydrochloride.

587

588 Therefore, unravelling new integrated rate-laws for more extended photdegradation
589 mechanisms, using the method previously developed (Maafi and Maafi, 2014), would certainly
590 shed more light on photodegradation kinetics and will open more opportunities to develop
591 robust drug-actinometers.

592

593

References

Al Omari, M.M., Zoubi, R.M., Hasan, E.I., Khader, T.Z., Badwan, A.A., 2007. Effect of light and heat on the stability of montelukast in solution and in its solid state. J. Pharm. Biomed. Ana. 45(3), 465-471.

Alsarra, I.A., 2004. Develeopment of a stability-indicating HPLC method for the determination of montelukast in tablets and human plasma and its applications to pharmacokinetic and stability studes. Saudi Pharm. J. 12(4), 136-142.

Arison, B.H., Baillie, T.A., Balani, S.K., Dufresne, C., 1999. US Patent Number 5,952,347, Application number US19980037949.

Baertschi, S.W., Alsante, K.M., Tonnesen, H.H., 2010. A critical assessment of the ICH guideline on photostability testing of new drug substances and products (Q1B): recommendation for revision. J. Pharm. Sci. 99, 2934-2940.

Baertschi, S.W., 1997. Commentary on the quinine actinometry system described in the ICH draft guideline on photostability testing of new drug substances and products.Drug Stability. 1, 193-195.

Challa, B.R., Awen, B., Chandu, B.R., Khagga, M., Kotthapalli, C.B., 2010. Method development and validation of montelukast in human plasma by HPLC coupled with ESI-MS/MS: Application to a bioequivalence study. Scientia Pharmaceutica. 78, 411-422.

De Azevedo Filho, C.A., De Filgueiras Gomes, D., De Melo Guedes, J.P., Batista, R. M. F., Santos, B.S., 2011. Considerations on the quinine actinometry calibration method used in photostability testing of pharmaceuticals. J. of Pharm. and Biomed. Anal. 54, 886-888.

Feliciano, M., Vytla, D., Medeiros, K.A., Chambers, J.J., 2010. The $GABA_A$ receptor as a target for photochromic molecules. Bioorg. & Med. Chem. 18, 7731-7738.

Fomina, N., Sankaranarayanan, J., Almutairi, A., 2012. Photochemical mechasnisms of light-triggered release from nanocarriers. Advanced Drug Delivery Reviews. 64, 1005-1020.

ICH, 1996. Guidance for industry Q1B photostability testing of new drug substances and products. Fed. Regist. 62, 27115-27112.

Kester, T.C., Zhan, Z., Bergstrom, D.H., 1996. Quinine actinometry studies under two light sources specified by the ICH guideline on photostability testing. Seattle, Washington. Presented at the AAPS National Meeting.

Maafi, M., 2010. The potential of AB(1) systems for direct actinometry. Diarylethenes as successful actimometers for the visible range. Phys. Chem. Chem. Phys. 12, 13248–13254.

Maafi, M., Brown, R.G., 2005a. General analytical solutions for the kinetics of AB(k, Φ) and ABC(k, Φ) systems. Int. J. Chem. Kinet. 37(3), 162-174.

Maafi, M., Brown, R.G., 2005b. Analysis of diarylnaphthopyran kinetics. Degeneracy of the kinetic solution. Int. J. Chem. Kinet. 37, 717-727.

Maafi, M., Brown, R.G., 2008. A fundamental system of equations to describe ABC(3k, 6Φ) dynamics. A contribution to the elucidation of [2H]-naphthopyran kinetics. Int. J. Chem. Kinet. 40, 268-281.

Maafi, W., Maafi, M., 2013. Modelling Nifedipine Photodegradation, Photostability and Actinometric Properties. Int. J. Pharm. 456(1), 153-164.

Maafi, M., Maafi, W., 2014. Φ-order kinetics of photoreversible drug reactions. Int. J. Pharm. Under consideration.

Ming, L., 2012. Organic Chemistry of drug degradation. RSC Drug Discovery Series No.29. The Royal Society of Chemistry, Cambridge.

Piechocki, J.T., Thoma, K., 2010. Pharmaceutical Photostability and Photostabilisation Technology. Informa Healthcare, London.

Radhakrishna, T., Narasaraju, A., Ramakrishna, M., Satyanarayana, A., 2003. Simultaneous determination of montelukast and loratadine by HPLC and derivative spectrophotometric methods. J. Pharm. Biomed. Anal. 31, 359-368.

Ricci, A, Fasani, E., Mella, M., Albini, A., 2003. General patterns in the photochemistry of pregna-1,4-dien-3,20-diones. J. Org. Chem. 68, 4361-4366.

Ricci, A, Fasani, E., Mella, M., Albini, A., 2001. Noncommunicating photoreaction paths in some pregna-1,4-dien-3,20-diones. J. Org. Chem. 66, 8086-8093.

Roman, J., Breier, A.R., Steppe, M., 2011. Stability indicating LC method to determination of sodium montelukast in pharmaceutical dosage form and its photodegradation kinetics. J. Chromato. Sci. 49, 540-546.

Smith, G.A., Rawls, C.M., Kunka, R.L., 2004. An automated method for the determination of montelukast in human plasma using dual-column HPLC analysis and peak height summation of the parent compound and its photodegradation product. Pharm. Res. 21(9), 1539-1544.

Schoors, D.F., De Smet, M., Reiss, T., Margolskee, D., Cheng, H., Larson, P., Amin, R., Somers, G., 1995. Single dose pharmacokinetics, safety and tolerability of MK-0476, a new leukotriene D4-receptor antagonist, in healthy volunteers. Br. J. Clin. Pharmacol. 40(3):277-80.

Thibert, R., Mach, H., Clas, S. D., Meisner, D.R., Vadas, E.B., 1996. Characterization of the self-association properties of a leukotriene D_4 receptor antagonist, MK-0476. Int. J. Pharm. 134, 59-70.

Tomatsu, I., Peng, K., Kros, A., 2011. Photoresponsive hydrogels for biomedical applications. Advanced Drug Delivery Reviews. 63, 1257-1266.

Tonnesen, H.H., **2004**. Photostability of Drugs and Drug Formulations (second Edition). CRC Press: London; 2004.

Wohl, B.M., Engebersen, J.F.J., 2012. Responsive layer-by-layer materials for drug delivery. Journal of Controlled Release. 158, 2-14.

Zhao, J.J., Rogers, J.D., Holland, S.D., Larson, P., Amin, R.D., Haesen, R., Freeman, A., Seiberling, M., Merz, M., Cheng, H., 1997. Pharmacokinetics and bioavailability of montelukast sodium (MK-0476) in healthy young and elderly volunteers. Biopharm. Drug Dispos. 18, 769-777.